On the detection of mesospheric meteoric smoke particles embedded in noctilucent cloud particles with rocket-borne dust probes

T. Antonsen[a] and O. Havnes
Department of Physics and Technology, University of Tromsø, NO-9037 Tromsø, Norway

(Received 26 June 2014; accepted 25 February 2015; published online 20 March 2015)

Mesospheric nanoparticles in the forms of water ice particles and meteoric smoke particles (MSPs) exist in the middle atmosphere where they often play a decisive role in cloud formation and in chemical processes. Direct *in situ* observations of mesospheric nanoparticles have been made possible by rocket probes developed during the last two decades. Although progress has been made in mapping properties such as electric charge, sizes, and interaction with the plasma and neutral gas, more observations are needed on the size distribution, chemical content, and structure of the MSP to determine their role in cloud formation and chemistry in the mesosphere and stratosphere. We here present the result of a detailed analysis of the performance of a new dust probe MUltiple Dust Detector (MUDD) [O. Havnes *et al.*, J. Atmos Soll.-Terr. Phys. **118**, 190 (2014); O. Havenes *et al.*, *ibid.* (in press)], which should give information of the size distribution of MSP by fragmenting impacting ice particles and releasing a fraction of the MSP which most probably are embedded in them [O. Havnes and L. I. Naesheim, Ann. Geophys. **25**, 623 (2007); M. E. Hervig *et al.*, J. Atmos. Sol.-Terr. Phys. **84-85**, 1 (2012)]. We first determine the electric field structure and neutral gas condition in the interior of the probe and from this compute, the dynamics and current contribution of the charged fragments to the currents measured as the probe scans the fragment energy. For the single MUDD probe flown in July 2011 on the PHOCUS payload, we find that the fragment currents at the three retarding potentials for MUDD of 0, 10, and 20 V correspond to fragment sizes of $\gtrsim$0.6 nm, >1.5 nm, and >1.8 nm if the fragments have a negative unit charge. We also discuss the optimum choice of retarding potentials in future flights of MUDD probes. By launching 2 to 3 mechanically identical MUDD probes but with different retarding potentials, we will obtain a much more detailed and reliable fragment (MSP) size distribution. © *2015 AIP Publishing LLC.* [http://dx.doi.org/10.1063/1.4914394]

I. INTRODUCTION

Dust particles, or aerosols, are abundant throughout the entire terrestrial atmosphere. In the high latitude mesosphere, at heights between ~80 and 90 km, dust or ice particles are found mainly in the form of nanoscale ice grains which can be optically detected as noctilucent clouds (NLCs)[5,6] or their related sub-visual phenomenon, polar mesospheric summer echoes (PMSEs).[7,8] A common factor of many of these studies is the connection between the icy dust forms and meteoric smoke particles (MSPs) which are discussed in more depth below.

The mesospheric dust has received a considerable amount of attention over the last couple of decades, much because of the implications they are suggested to have for the middle atmosphere chemistry. Strong evidence exists for the effective depletion of Potassium (K) and Sodium (Na) layers in the presence of icy dust particles.[9,10] The direction of the polar middle atmosphere wind draught is upwards during the summer and is thought to be important for the rapid growth of NLC particles. During winter, the wind draught changes direction and dust can acquire momentum downwards.[11–13] At lower altitudes, dust particles supply surface area where chemical reactions both indirectly and directly can remove ozone.[14,15] The temperature in the mesosphere has sunk $O(1)$ K since 1979, with cooling rates up to 0.4 Kyr^{-1}.[16,17] This offers an explanation for the significant increase in NLC frequency since 1979.[18,19] Mesospheric dust has moreover been suggested to indicate changes in the climate;[20,21] however, such capabilities have been challenged.[22]

Basic research on nucleation and growth mechanisms, the complex chemistry of the particles and their possible connection with neighboring atmospheric layers are other fields which are constrained by the limitations of observational studies. In the troposphere, long-time measurements by balloon and *in situ* measurements by airplane are much used techniques (see, e.g., Cziczo, Thomson, and Murphy[23] and Bigg[24] for recent reviews); however, these methods cannot be applied for mesospheric probing. Indirect remote methods such as ground based and space borne radar may be used, but have limitations. For this reason, rockets have become indispensable for mesosphere research as it is the only method which allows for *in-situ* operation. In addition, the sensitivity of rocket instrumentation is far superior of that of remote methods making the rocket the only tool to probe small scale phenomena.

Since the first direct evidence for charged particles in the mesosphere was presented by Havnes *et al.*,[25] a faraday cup design such as their DUSTY probe has often been the basic design for attempts of *in situ* measurement of various dust and aerosol particles. Gelinas *et al.*,[26] Lynch *et al.*,[27] and Rapp *et al.*[28] all used modified designs to successfully detect charged

[a]Electronic mail: tarjei.antonsen@uit.no

particles in the mesosphere. These studies represent important steps towards an experimental verification of theoretical MSP size distributions and charge state. *In situ* studies, such as the previous, have confirmed the elusive nature of MSPs and have pointed out problems with decisively determining their characteristics. By using alternative mass spectrometer designs, Schulte and Arnold[29] and Robertson *et al.*[30] detected aerosols with sizes of up to a few nanometers in the mesosphere. A major problem for MSP detection experiments is that particles at their sizes tend to be swept away from rocket probes by the airflow around them.[31,32] This greatly complicates the utilization of faraday cup designs. However, recent observations and new considerations presented in this paper that NLC particles probably contain a significant number of embedded MSPs which suggest that a simple cup design can indeed be used to detect MSPs.

The daily mass influx of meteoric material into the middle atmosphere is generally thought to be on the order of 1–100 metric tons (Love and Brownlee;[33] see Plane[34] for a recent review). The majority of the meteoric ablation occurs in the height range between 70 and 110 km where they deposit layers of atomic metals.[35,36] Rosinski and Snow[37] proposed early that the oxidization of ablation vapor could create species such as iron oxide (FeO) and silicon oxides (SiO/SiO_2) which were likely to subsequently re-condense into nanometer-scale solid particles, so called MSPs. This work was further developed by Hunten, Turco, and Toon[38] who introduced a microphysical model considering not only the initial re-condensation, but also subsequent growth of the particles by coagulation, and particle transport by eddy-diffusion. The calculations in the latter work predicted number densities of MSPs up to several thousand cm^{-3} for sizes up to a few nanometers.

The chemical composition of these smoke particles has been discussed since their theorization. Current studies from both laboratory and remote measurements by satellite have proposed compositions consistent with a chondritic origin.[4,39] Moreover, electron structure theory has been used to justify that metal silicates with large dipole moments should form in the mesosphere and subsequently, act as efficient nucleation sites for water to form icy dust particles.[40] This latter work extends the view that MSPs are the most likely nuclei for mesospheric ice particles (see Rapp and Thomas[41] for a detailed review) to a nuclei of few or single molecules of meteoric origin. Early models of NLC particle nucleation relied on the idea that NLCs contained cores of single MSPs and had few other contaminants in the ice layer,[42] a view that was withheld for a long time and even backed up by experiments.[6,43] However, impurities such as molecules of meteoric origin and larger MSPs may amplify the growth significantly by lowering the surface energy barrier for nucleation.[44,45] On the basis of rocket measurements and modeling, Havnes and Næsheim[3] shifted this view of the traditional NLC particle towards an ice dust particle with *many* embedded MSPs, uniformly distributed as the different nucleation and growth mechanisms compete until a depletion of the local water density. Recently, this embedded MSP prediction has obtained further support from satellite observations,[4] which estimates a volume filling factor of meteoric material between 0.01% and 3% in dust from polar mesospheric clouds (PMCs). It should be noted, however, that by modeling the global MSP distribution, Megner *et al.*[46,47] found that the concentrations of MSPs at the polar summer mesopause were not high enough to account for the high number density of the NLC particles alone, opening for the ongoing discussion on NLC nucleation and growth mechanisms and MSP transport. Those works propose that a pure heterogeneous mechanism may be insufficient for explaining nucleation, but that free smoke particles can be effective nuclei when accompanied by moderate temperature gradients. This could significantly increase the number of available nucleation sites compared to a situation where MSP of sizes ~1 nm was required for condensation into larger ice particles. Homogeneous mechanisms, where the mesospheric water vapor condenses to amorphous and even solid states, have furthermore been shown to compete with heterogenous nucleation when the temperature gradient is moderately negative, as can be the case in temporarily strong cooling forced by gravity waves propagating upwards.[44,48] Measurements of NLC particle radii have been found to be consistent with a mean of around 50 nm for a monodispersive distribution and shifted downwards for polydisperse distributions.[49–51] These "large" particles must therefore have grown substantially, even if the initial nucleus was a MSP with a radius in the upper tail of their theoretical size distribution (see Hunten, Turco, and Toon[38] and Megner, Rapp, and Gumbel[52]).

The present paper aims to utilize the "new" NLC particle and simulate the dynamics of its fragments inside a bucket probe. For this purpose, we use the MUDD probe (MUltiple Dust Detector) which was developed at the University of Tromsø and flown in the PHOCUS campaign in July 2011, as our simulation domain. Several studies have found that dust particles colliding with surfaces on rockets will rub off secondary charges, a process which in some cases has been found to dominate the recorded signal.[3,25,53–55] It has been argued[1,3,55] that the large secondary production is mainly caused by the presence of the embedded MSPs which will not evaporate even if similarly small ice particles would. The majority of the smallest fragments may therefore reflect the true size distribution of MSPs. We report the results of modeling collision fragment motion and current contribution to the grids inside bucket dust probes similar to the DUSTY probe.[25] The motion is calculated on basis of E-field and neutral gas condition simulations. The numerical model we have developed is aimed at being used both to improve the analysis of results from MUDD probes which have been, and will be, launched and to assist in developing new rocket probes for measuring dust in the mesosphere. The MUDD probe[1,2] is nearly identical to the DUSTY probe except that its lowest grid (G2) is made up of concentric inclined strips. Due to this, no ambient dust particle entering the probe can pass and directly hit the bottom plate of the probe. They will all hit G2 and we expect the majority of the icy NLC/PMSE particles to partly fragment and that many of the fragments will rub off charge from G2 and carry them to the bottom plate. We do not expect "free" MSP, which are not embedded into NLC/PMSE particles, to contribute significantly to the currents measured at the bottom plate of MUDD. The majority of such "free" MSP, having sizes below ~2 nm, will be carried away from the

probe by the airstream around the payload. Larger MSP may enter the probe, but for sizes up to ~5 nm, the impact velocities will be low, resulting in a low probability for charging, or in attachment to the impact grid G2.

In Sec. II, we present the technical details of the MUDD detector. Section III is dedicated to our theoretical model, including E-field simulations, neutral gas simulations, and charged dust dynamics. The model equations for transport and evaporation of dust particles and the closure of these based on static background simulations are presented. The results from our simulations of pure MSP fragments and pure ice fragments resulting from the collision of NLC particles in MUDD are presented in Sec. IV. A discussion is given in Sec. V.

II. THE MUDD PROBE

Figure 1 shows a principle sketch of the MUDD probe, which is an augmentation of the original bucket design of Havnes *et al.*[25] The detector is a faraday cup with two biased square meshes, G0 and G1, and a lower biased fragmentation grid, G2, which consists of partly overlapped inclined (≈20° with normal) concentric rings, allowing for no direct dust particle influx to the bottom detector plate, BP. The uppermost grid, G0, is set to the rocket payload potential; ideally at 0 V, however, rocket payloads often acquire small negative voltages during flight.[56] Small bias voltages on the probe (~1 V) will not significantly affect the grid voltages, as the grids are isolated from the payload, and the field from the probe walls does not affect the vertical motion of fragments. The G1 grid is biased to a constant value of +6.2 V, which will shield out ambient positive ions, while electrons may pass. The ion flux can be affected by boundary E-field effects, as will be discussed. The dust particles which hit G2 are mainly NLC or PMSE particles, and their fragments will move towards BP if they are not stopped by the electric field or neutral gas drag. "Free" MSP particles in the ambient dust population are either deflected away from the MUDD probe or, if entering it, they are broken so much that their probability for charging is very low, or they attach to G2. They do not contribute significantly to the current at BP. G2 has a constant voltage of +10 V, while BP alternates between +10 V, 0 V, −10 V, and back to 0 V and then repeats this cycle. Details on the sampling scheme for the MUDD probe launched in 2011 can be found in Havnes *et al.*[1] The BP current sampling frequency was then 1920 Hz, but the scheme will be improved for the launch of MaxiDusty-I. The electric field—and retarding potential—is zero between BP and G2 for the mode in which V_{BP} = 10 V. This mode measures all charged fragments which are not stopped by neutral drag and will also measure the current of a significant number of free electrons for which a correction must be made.[1,2] In regions where dust is absent, this electron "leakage" current is the only contribution to BP. The other voltage modes of retarding potentials 10 V and 20 V will not measure free electron current, as they are stopped by the electric fields. By altering the G2-BP E-fields, fragments from different regions of the energy spectrum will hit BP, and this study is concerned with how to obtain a fragment size distribution from the measured currents.

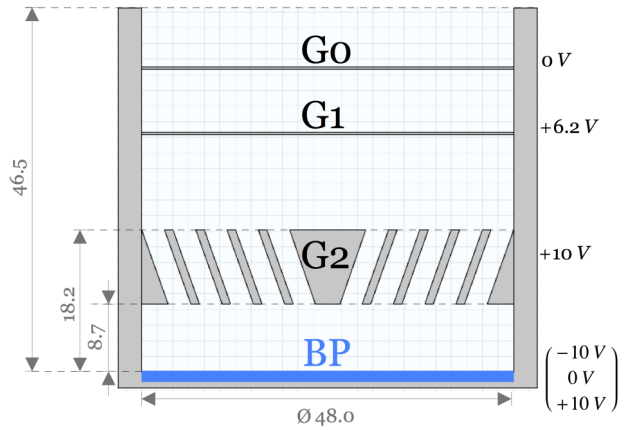

FIG. 1. Vertical cross section of the MUDD probe. Length measures are in millimeters.

III. MODELING

In our efforts to solve the problem of single dust fragment dynamics inside MUDD, we present a model based on parameters from different background simulations. We have split the modeling into three parts: electric field structure, neutral gas field fields, and charged dust grain dynamics including heating and evaporation. The E-field and neutral gas simulations are used as static inputs for the dust simulations.[57] The neutral gas and dust calculations are presented in Secs. III A and III B below. The E-field simulations will not be addressed in depth here. A FEM-procedure solving Poisson's equation in radial symmetry from COMSOL[57] was used to calculate the different field configurations for the rotational symmetric MUDD probe. The E-field configuration for the case when the BP voltage is $V_{BP} = -10V$, i.e., the mode of largest retarding potential which will detect the highest energy particles, is presented in Fig. 2.

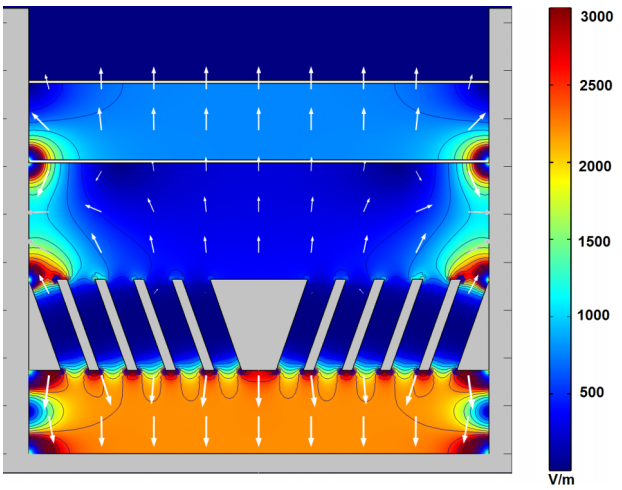

FIG. 2. Electric field in Vm^{-1} inside MUDD for a bottom plate potential of −10 V. The field values are cutoff at 3000 V/m, although the fields around sharp edges can be a factor of 10 larger than this; however, this effect is very local.

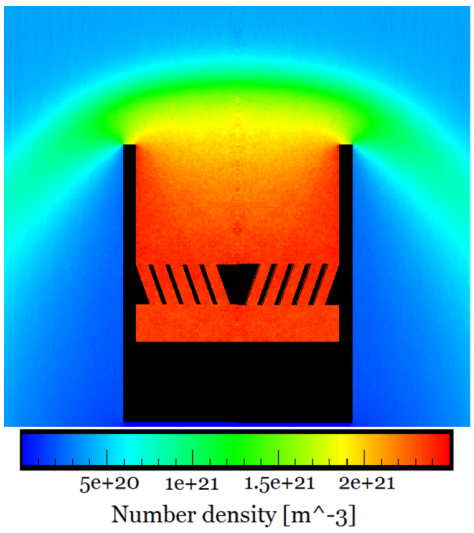

FIG. 3. Simulated neutral gas number density around MUDD at 82 km altitude, for $v_r = 750$ ms^{-1}.

A. Neutral gas fields

The degree to which a gas is rarefied can be quantified by the dimensionless Knudsen number, Kn, defined as the ratio of the mean free path of undisturbed flight of a gas molecule to a characteristic dimension, e.g., an instrument dimension or dust radius, of a system,

$$Kn = \frac{\lambda_{mfp}}{L}. \tag{1}$$

For a typical dust bucket probe, i.e., $L \sim 0.1$ m, inside and in the vicinity of rocket probes during operation in the mesosphere, the mean free path is large enough so that the collision derivative in Boltzmann's transport equation is not well defined. The continuous flow Navier-Stokes equations or other modified versions of Boltzmann's equation can thus not be used to derive neutral gas fields inside the probe.[58] The solution is to treat the gas flow with probabilistic methods; the Direct Simulation Monte Carlo (DSMC) method proposed by G. Bird (described in Bird[59]) to obtain quasi-steady solutions. We will in this study use the DS2V code written by Bird to treat the problem in rotational symmetry, searching for steady flows at large times. The flow fields are subsequently used as input to the dust fragment simulations and is shown in Fig. 3.

B. Dust dynamics

The relatively low ambient gas density in the height region of NLCs, generally between 80 and 90 km, ensures that the compressed air outside, in front and inside of a bucket probe is dominated by transitional flow Knudsen numbers (~0.01 – 1 for our system). For the neutral gas-dust drag force, we therefore use an expression modified for this regime, valid for sub- and supersonic dust speeds, assuming a specular reflection of neutrals in a collision with a dust grain,[60,61]

$$\mathbf{F}_{gd} = \chi \pi r_d^2 m_g n_g v_{th,g} (\mathbf{v}_g - \mathbf{v}_d) \frac{1}{u} \left\{ \frac{1}{\sqrt{\pi}} \left(u + \frac{1}{2u} \right) \exp(-u^2) + \left(1 + u^2 - \frac{1}{4u^2} \right) \mathrm{erf}(u) \right\}, \tag{2}$$

where r_d and $\mathbf{v}_d$ are the dust fragment radius and velocity, respectively; $m_g, n_g, \mathbf{v}_g$, and $v_{th,g} = (2k_B T_g/m_g)^{\frac{1}{2}}$ are the local neutral gas parameters, and $u = |\mathbf{v}_g - \mathbf{v}_d|/v_{th,g}$ is the relative Mach number of the dust particles. The factor $\chi = F_{gd}^p / F_{gd}^{ve}$ is the dynamic shape factor defined as the ratio of the neutral air drag on a non-spherical particle to the drag introduced by its volume equivalent sphere.[62] This correction factor is useful for modeling dynamics of non-spherical agglomerates, but its dependence of particle orientation, flow regime, and particle size can introduce uncertainties.[63]

When ignoring incoming radiation and thermal emission, as motivated by the finding of Rizk, Hunten, and Engel[64] that sub-micron particles of meteoric origin tend to not radiate away heat easily, the energy balance energy equation becomes[31,61]

$$\begin{aligned} \hat{P}_N &= \frac{\pi}{4} r_d^2 n_g v_{th,g} k_B T_g \left\{ \frac{2}{\sqrt{\pi}} \left[5 + 2u^2 \right] \exp(-u^2) + \frac{1}{\sqrt{u^2}} \left[3 + 12u^2 + 4u^4 \right] \mathrm{erf}(u) \right\} \\ &= \frac{4\pi}{3} \rho_d r_d^3 c_p \frac{dT_d}{dt} + L_d \frac{dm_d}{dt}, \end{aligned} \tag{3}$$

where ρ_d, m_d, and L_d are the mass density, mass, and latent heat of evaporation of a dust grain, respectively; c_p denotes the specific heat of the dust grains. The numeric values of the parameters used in the simulations are summarized in Table I. The expression denoted $\hat{P}_N$ on the lhs is the heating power of dust grains due to collisions with neutrals modified for

TABLE I. The basic set of dust parameters used in the simulations.

Parameter	Value	Note
MSP mass density, ρ_s	3000 kgm^{-3}	Plane,[40] Klekociuk *et al.*[80]
Ice mass density, ρ_i	980 kgm^{-3}	
Fragment charge, q_d	−1 e	Discussed in Sec. III C
Mean dust weight, m_D	140/18 a.m.u.	For MSP/ice, respectively
Initial fragment velocity, v_0	450 ms^{-1}	Tomsic[68]
Latent heat of vaporization of ice, L^{ice}	2.78×10^6 J kg^{-1}	Lichtenegger and Kömle[81]
Latent heat of vaporization of MSP, L^{smoke}	6×10^6 J kg^{-1}	Hunten, Turco, and Toon[38]
Specific heat of ice, c_p^i	$90+7.5T_d$ J kg^{-1}K^{-1}	Klinger[82]
Specific heat of smoke, c_p^s	1000 J kg^{-1}K^{-1}	Hunten, Turco, and Toon[38]
Mean surface energy of smoke, $\bar{\gamma}_{smoke}$	0.200 J m^{-2}	Gundlach *et al.*[83]
Surface energy of ice, γ_{ice}	0.190 J m^{-2}	Heim *et al.*[84]

diffusive reflection of the neutral gas molecules which leave with the characteristic temperature of the dust.[61] The rhs terms originate from the heat due to increased temperature and the heat loss due to vaporization of the grain, respectively.

By assuming local thermodynamic equilibrium and that surface molecules leave diffusively from the dust grain, we can express the rate of change in radius as a function of intrinsic dust properties (cf. Evans[45]),

$$\frac{\mathrm{d}r_d}{\mathrm{d}t} = -\frac{P_{vap}(T_d,r_d)}{\rho_d}\left(\frac{m_D}{2\pi k_B T_d}\right)^{\frac{1}{2}}, \tag{4}$$

where $P_{vap}(T_d,r_d)$ is the material specific vapor pressure, m_D is the mass of *one* dust surface molecule, and ρ_d is the grain density.

Podolak, Pollack, and Reynolds[65] give the vapor pressure terms for ice and MSP-like components as

$$P_{vap}(T_d) = \begin{cases} 3.89\cdot 10^{10}\exp\left(-4845/T_d\right) & \text{for ice} \\ 1.51\cdot 10^{12}\exp\left(-56655/T_d\right) & \text{for smoke} \end{cases}. \tag{5}$$

However, we must correct this for very small surfaces. The term which allows for spherical ejection of material from small bodies is given in Evans[45] as

$$P_{vap}(T_d,r_d) = P_{vap}(T_d)\cdot\exp\left(\frac{2\gamma m_D}{\rho_d k_B T_d r_d}\right), \tag{6}$$

where $P_{vap}(T_d)$ is the term from Eq. (5), and γ is the specific surface energy of the dust grain.

We calculate the dust grain temperature self-consistently from Eq. (3) by rewriting the mass derivative,

$$\frac{\mathrm{d}T_d}{\mathrm{d}t} = \frac{\hat{P}_N - L_d\cdot 4\pi r_d^2\left(\frac{m_D}{2\pi k_B T_d}\right)^{\frac{1}{2}}\cdot P_{vap}(T_d,r_d)}{\frac{4\pi}{3}\rho_d r_d^3 c_p}. \tag{7}$$

Neutral gas field solutions from the DSMC simulations as well as electric field solutions and dust material specific parameters were used to close the model equations for single dust particle movement. Most emphasis was put on the movement of single charged fragments, as NLC particles are expected to be partly crushed and that fragments are ejected from the concentric rings of G2. This process is discussed in more detail in Sec. V A. In Figure 4, we present typical results from the idealized situation where the fragmentation at one of the inclined concentric rings is considered. The local deviation from a homogeneous electric field between G2 and BP and inside G2 was neglected. The particles were traced from the point of fragmentation through a certain integration time, until their radii were reduced to 1 Å or until they hit a system boundary. A larger fraction of the 1.6 nm radius MSP trajectories (Fig. 4, top) hits BP compared to the 3 nm pure ice particle trajectories (54% vs. 38%). The ice particles experience a much larger neutral gas friction, as well as evaporation due to their intrinsic properties which leads to that relatively large ice particles would contribute less to the measured current at BP than MSPs in the upper part of the theoretical size distribution, as will be discussed in depth below.

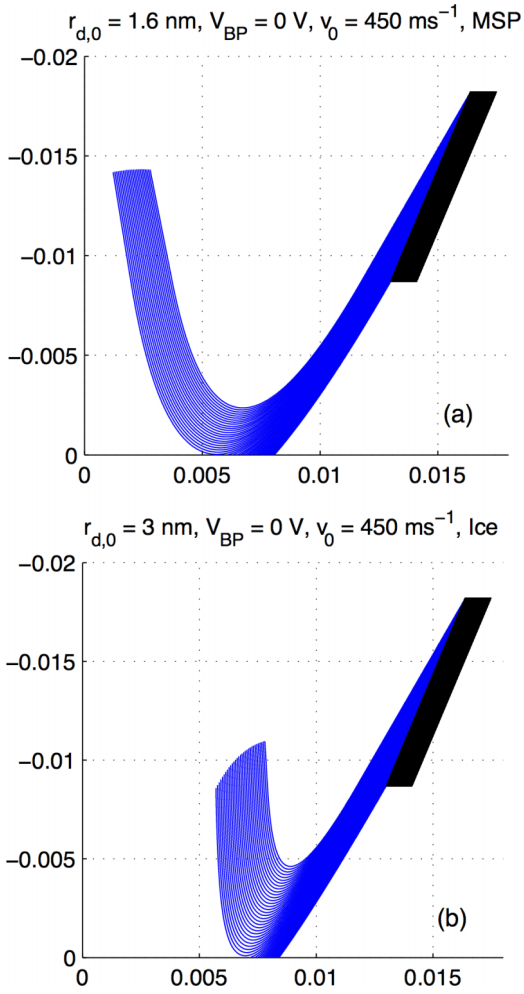

FIG. 4. Traced trajectories (blue solid lines) of 1.6 nm radius MSPs (top) and 3.0 nm pure ice particles (bottom) for a bottom plate potential of 0 V. The black structure is a cross section of one inclined ring in G2. The y-axis and x-axis give the vertical and (arbitrary) radial position from the center of the probe, of the ring and the fragment orbits. Units are (m).

C. Choice of dust parameters

The calculations performed in this work require knowledge about a range of intrinsic dust properties to close the model equations. To find recent, or even any, material specific data which apply to MSPs can be a challenge due to the limited knowledge of their chemistry. This issue is often resolved by using data from analogues of smoke particles, and we summarize the set of dust parameters used in this study in Table I. A few comments on the choices of MSP parameters should however be made.

The MSP material density is often assigned a value of $\rho_d = 2000$ kg m^{-3}.[38,46,66,67] However, on the basis of both observations (e.g., Hervig *et al.*[4]) and theoretical discussions (see, e.g., references listed in Table I), this number may be too low. If the MSPs are indeed formed from chondritic material, the density could be at least $\rho_d = 3000$ kg m^{-3} as set here (non-stoichiometric olivine compound), and possibly higher, even for amorphous states.

The choice of initial velocity for the fragments at G2 in MUDD, $v_0 = 450$ ms^{-1} for a rocket velocity of around $v_r = 750$ ms^{-1}, is the parameter containing the largest uncertainty

at this point. The collision dynamics of nanoparticles is not very well known, and our assumptions about nanoscale ice particles are based on studies by Tomsic,[68] Tomsic, Marković, and Pettersson,[69] Tomsic *et al.*,[70,71] and Andersson *et al.*[72] of impacting pure ice particles. For nanoscale ice particles, their experiments show that $O(100)$ eV-particles may conserve up to 70% of their initial energy when colliding with gold or graphite coated surfaces at an incident angle of 70°. Extrapolating these results to lower energy particles gives a conservation of around 40% of the initial energy, on which we have appended an uncertainty of $\pm 100\ \mathrm{ms}^{-1}$ (corresponding to ~36% ± 15%). This energy loss is valid for pure ice particles; however, it is conceivable that the energy loss for the MSPs will be similar to the characteristic one for ice particles, if they are embedded within or bounded on the surface of, e.g., a NLC particle. Sato, Chen, and Pui[73] also find that silica, silver, and nickel nanoparticles colliding with silver surfaces lose a large amount of their perpendicular velocity. We find it conceivable that the MSPs, unlike many ice particles, will keep much of their velocity parallel to the surface due to, e.g., lubrication by water layers.

The charge state of the fragments should be discussed. As noted by Kuuluvainen *et al.*,[74] the transfer of charge to nanoparticles impacting on surfaces as well as their bouncing properties is not well understood. In studies of pure ice particles,[68–72] it is found that surface impacts of smaller particles generally lead to that they stick to the surface and evaporate while larger particles bounce off and appear to be more or less intact. Such a scenario cannot explain the large production of charged fragments which has been observed in several rocket experiments,[1,3,55] where the secondary charge production in a triboelectric mechanism corresponds to that a particle of radius 50 nm should produce between 50 and 100 charged fragments, while a smaller particle of radius say 10 nm produces around five charged fragments. It is not likely that all released fragments are charged. In moderate to high energy collisions of ice particles[68,75,76] and MSP-like particles[77] with metal surfaces, it is found that the particles can break into fragments of which a proportion ($\sim 0.01\% - 0.1\%$) become charged, a probability proportional to $m_{ice}^{2/3}$ and m_{MSP}, respectively. The discrepancy between these results and those from rocket experiments points towards a structure of NLC/PMSE particles which is more loosely bound than a pure ice particle. It seems likely that the effect of a large number of embedded MSPs[1,3,4] could lead to just this. The fact that so many of the small fragments from impacting NLC/PMSE particles do not stick to the impact surface, as similar ice particles tend to do, also suggests that their velocity can be larger than what we find for ice particles at the relevant energies for the MUDD observations. For very small dually or more strongly charged particles, the electric potential at the surface can, depending on the material, exceed the surface tensile potential.[78] In view of that the probability for a fragment to acquire one unit charge is less than unity, possibly considerably so, we find the assumption that fragments at most carry one unit charge to be reasonable. We also assume that the majority of fragments will have a negative charge, as is observed during the first minutes of exposure of a metal surface to impacting nanoscale ice particles.[68] Two unit charges can probably not be totally excluded, but it seems very unlikely that such fragments can carry a substantial fraction of the BP current. It may also be that electric field emission prevents the existence of two or more unit charges on dust particles of the order of one nm radius.[79]

It is assumed throughout this study that the ejection angle of a fragment is 6° to the G2 surface, based on results for ice particles of similar size (e.g., Tomsic[68]) which show that fragments scatter diffusively around angles very close to the collision surface at our inclination angles, although uncertainty may be present in this parameter. We do not expect this to have large effect on the results, as small deviations around this angle is found to introduce around 2% more or less hits per degree for typical fragment sizes.

IV. RESULTS FROM FRAGMENT SIMULATIONS

Neutral gas simulations were performed for the polar summer mesosphere with density data from Rapp, Gumbel, and Lübken.[85] Calculations were carried out for an assumed altitude of 82 km and an ambient temperature of $T = 150$ K.[86] This is consistent with the observed NLC height during the PHOCUS campaign.[1] Dust simulations were run for single dust fragments which were singly charged. For each chosen dust radius, we simulated the motion of 50 fragments, with initial coordinates evenly spaced over the entire G2 fragmentation surface. A set of simulations of 50 nm NLC particles flowing in to the probe, through the shock front, was also performed. Those particles were found to preserve most of their initial energy, hitting G2 with a velocity just below $700\ \mathrm{ms}^{-1}$ which corresponds to around 85% of their initial energy. The sizes of the simulated fragments were chosen so that the maximum and minimum detectable radius in a specific voltage mode of MUDD was included.

Presented below are the main results from the simulation of pure MSPs and pure ice fragments in the original voltage modes of MUDD as flown on PHOCUS.[1] Simulations of alternative voltage modes to be used in future flights of MUDD probes are also presented.

A. MSP fragments

We now assume that the fragments, which are produced when PMSE/NLC particles hit G2, are pure MSP. For each set of 50 fragments with given radius and velocity, we calculate the fraction of them which will reach the bottom plate and contribute to the BP current. Figure 5 shows this as the relative current, for the two retarding potentials of 10 and 20 V corresponding to bottom plate potentials of 0 and −10 V. In the case of a bottom plate potential of $V_{BP} = 0$ V, i.e., a retarding field of approximately $1100\ \mathrm{Vm}^{-1}$, MSPs with radii as small as 1.4 nm can contribute to the BP current for an initial velocity of $450\ \mathrm{ms}^{-1}$ (solid line). All fragments larger than 1.8 nm will contribute to the current, and fragments with radii between around 1.4 nm and larger can be inferred with this mode. The adopted uncertainty in velocity shifts the smallest detectable radius down about 0.2 nm for a $100\ \mathrm{ms}^{-1}$ higher initial velocity, and up between 0.3 and 0.4 nm for the lower bound. The situation is very similar for

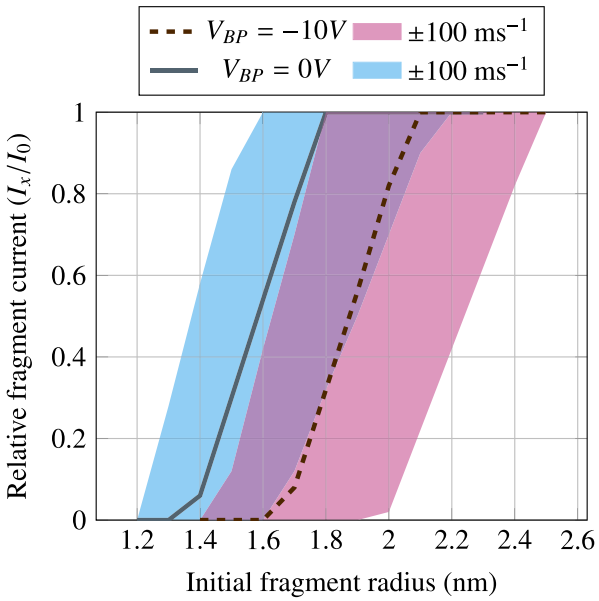

FIG. 5. Currents of pure MSP fragments at BP relative to the zero retarding field mode ($V_{BP} = +10$ V). The lines represent an initial velocity at G2 of $v_0 = 450$ ms^{-1}. I_x denotes the current at BP when $V_{BP} = x$ V.

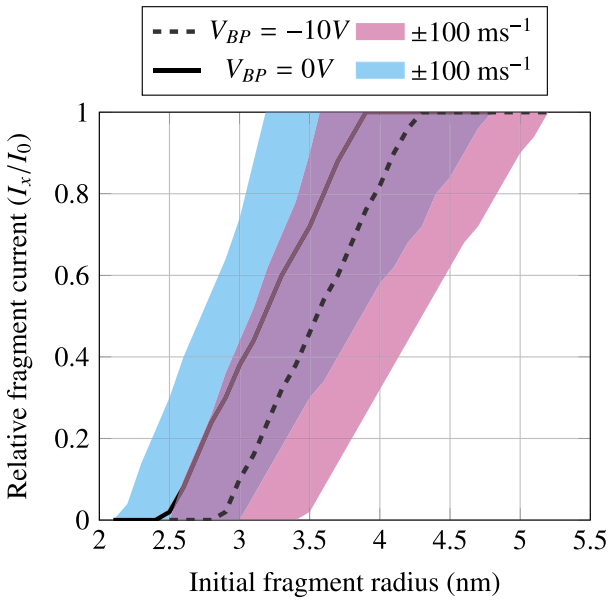

FIG. 6. Currents of pure ice fragments at BP relative to the mode with zero retarding potential.

the case when $V_{BP} = -10V$, i.e., a ≈2200 Vm^{-1} retarding field, where the 450 ms^{-1}-particles (dashed line) are theoretically detectable at radii above 1.7 nm. Particles larger than 2.1 nm will all reach the bottom plate, and the uncertainty in velocity shifts the distribution down around 0.2 nm or up 0.3 to 0.4 nm depending on the radius. In the mode, where there are no retarding fields, i.e., when $V_{BP} = 10$ V, our simulations show that MSP particles smaller than ~0.6 nm are stopped completely. In view of the assumed uncertainty in initial fragment velocity, this range becomes 0.5–0.8 nm. In reality, because of the MUDD geometry, small to moderate retarding fields can be present in this mode, which is discussed in Sec. V D. If we require that $I_x/I_0 \geq 30\%$ to detect the charged fragments, MUDD detects MPSs with sizes above ~1.5 nm in the 10 V retarding potential mode, and sizes above ~1.8 nm in the 20 V retarding potential mode. For the zero potential mode ($V_{BP} = +10$ V), MSPs larger than ~0.7 nm can contribute to the BP current, where the uncertainty in initial velocity will shift this limit down to 0.6 nm or up to 0.9 nm. All fragments larger than 0.9 nm are found to reach the bottom plate in the zero field mode.

B. Pure ice fragments

The results for simulations of pure ice fragments are presented in Figure 6 for retarding potentials of 10 V and 20 V between G2 and BP inside MUDD.

In the mode with a retarding potential of 10 V, we observe that particles with radii above 2.5 nm may contribute to the BP current if they are not obstructed at impact. The uncertainty in the smallest detectable radius is around 0.3 nm smaller and 0.5 nm larger than the mean (450 ms^{-1}-fragments). In the second voltage mode, where the retarding potential is 20 V, ice fragments with sizes above around 3 nm will contribute to the BP current. The uncertainty in detectable radius for this mode is slightly larger, 0.4 nm smaller and 0.6 nm larger than the mean value. As has been discussed, ice particles of sizes smaller than around 3 nm tend to stick to surfaces in collisions.[68] Combined with the small charging probability of these smaller ice fragments, they probably do not contribute significantly to the measured current at BP.

We find that the ice particles experience a significant evaporation within the integration time, typically ~$O(10^{-4})$ s. As shown in the bottom panel of Figure 7, a pure ice fragment of 3.5 nm can lose as much as 1/4 of their initial mass before hitting BP. This result, alongside simulations of MSPs with layers of ice a few Ångstrøm thick, supports that if ice were to stick to the MSP particles in the fragmentation process, this layer of ice would evaporate quickly and not distort the measured energy distribution of MSPs significantly. Although the MSPs are found to rapidly acquire heat, no significant evaporation is observed as can be inferred from the top panel of Fig. 7. We may also note that the breaking of these small fragments by neutral air can be substantial, resulting in a large difference in energy of the impacting fragments coming from the top and bottom of G2.

C. Alternative fragment detecting modes

Motivated by the goal of improving the resolution of the observed fragment energy spectrum, especially for lower energies, we present a summary of the simulations carried out for pure MSP fragments in voltage modes with lower retarding potentials.

Figure 8 shows a comparison between the three original potential modes and three additional modes at lower retarding potentials of 1V, 2V, and 5V, respectively. It shows the fraction of hits to BP by fragments of a certain energy (or size). Fragments with radii smaller than 1 nm can be detected both with the 1 V retarding mode ($V_{BP} = 9$ V) and the 2 V retarding mode ($V_{BP} = 8$ V). Inclusion of such low energy

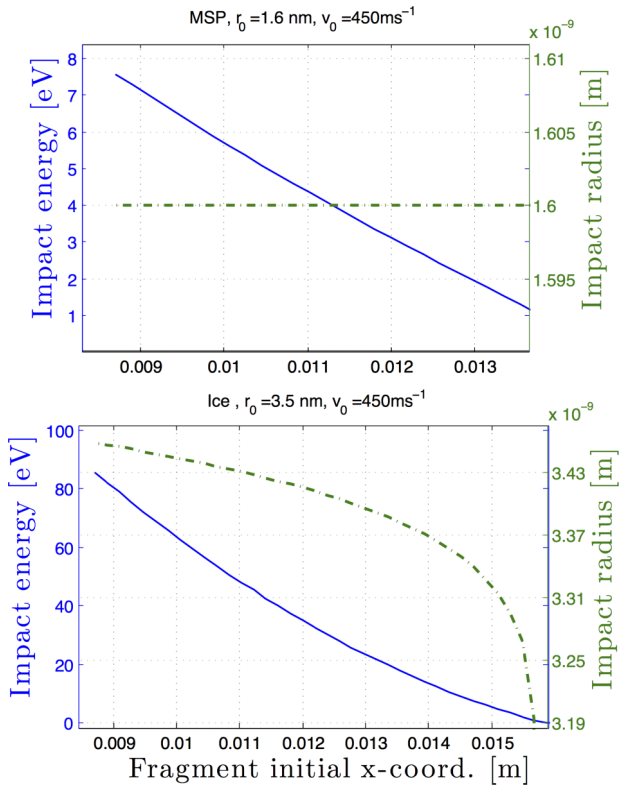

FIG. 7. Energy (solid line) and radius (dashed) at impact with BP for 1.6 nm radius MSP particles (top) and 3.5 nm pure ice particles (bottom) as a function of initial position.

modes should give a significantly increased resolution in the lower end of the fragment size spectrum, which can be related to the energy spectrum of MSPs, cf. the discussion in Sec. V C. To measure charged fragments with sizes which would normally be stopped by the air drag in the zero potential mode, we plan to include modes with small attractive potentials (e.g., $V_{BP} = +11$ V) as part of the voltage scheme in future flights of MUDD.

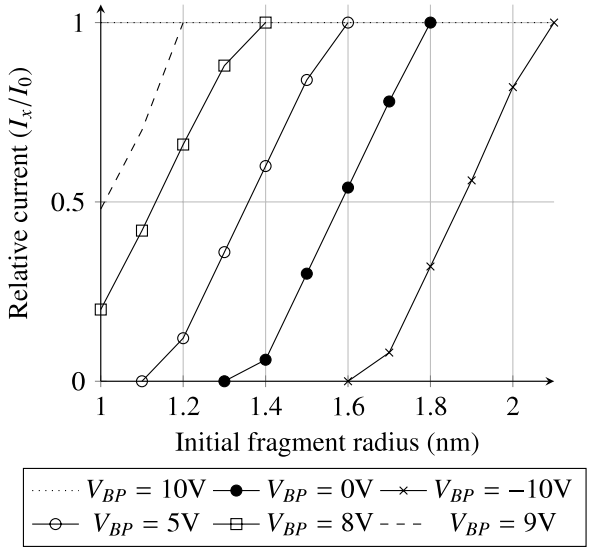

FIG. 8. Ratio between the current of the zero retarding potential mode and several modes with retarding potentials ($V_{BP} \neq 10$ V) for pure MSPs. The initial velocity is 450 ms^{-1}. I_x denotes the current at BP when $V_{BP} = x$ V.

V. DISCUSSION

A. Fragmentation process

Our model of a NLC particle is based on recent studies which show that they probably contain a relatively large amount—up to several percent by volume—of MSPs embedded in them.[1,3,4] There are, however, few experiments which apply directly to the collision and fragmentation dynamics of nanoparticles in a system like ours. Tomsic[68] presents experimental data and molecular dynamics simulations for collisions between ice particles down to a few nanometers and various surfaces. Their velocity regime is similar to ours, however, their experiments utilize collision surfaces with temperatures up to 1400 K, which is above what is relevant for our applications. Nevertheless, studies of lower temperature collisions (see, e.g., Tomsic *et al.*,[70] Andersson *et al.*,[72] and Markovic *et al.*[87]) show that the preservation of initial kinetic energy is very similar for low and high temperature collisions; however, in the latter case, the final energy spectrum tends to include a significant amount of low energy particles. In addition to this, Tomsic *et al.*[71] found that surfaces with temperatures ~300 K produce relatively narrow velocity distributions of the scattered fragments, so our uncertainty in initial fragment energy of about 30% will cover much of the variance. For low temperature collisions, Tomsic,[68] Tomsic, Marković, and Pettersson[69] find that small ($\lesssim$3 nm) water clusters tend to stick to the impact surfaces.

Kassa *et al.*[55] modeled the observations by different dust probes on the ECOMA-4 payload (see Rapp *et al.*[88] for details), where a probe with four times less geometric cross section than a larger one with similar geometry, could measure up to twice the current of the large probe. They found that this apparently had as an explanation that the smaller probe, located further back on the payload structure, was sprayed with collision fragments from ice particles impacting on the payload body in front and adjacent the smaller probe. The observations required that a 50 nm particle should produce between 50 and 100 charged fragments in a collision. A calculation based on the observations of MSP content by volume from Hervig *et al.*[4] and Havnes *et al.*,[1] shows that even if only the outermost layer of evenly distributed MSPs on a contact area equal to 1/4 of the dust surface area is released, then between 50 and 400 meteoric particles will be released if we assume a monodisperse distribution with $r_{MSP} = 1.4$ nm. Even if only a modest fraction of these become charged, they can contribute significantly to the total current (see also Havnes *et al.*[1]), thus reducing the requirement that the NLC particle itself is porous. However, the large difference in, e.g., specific heat between MSPs and ice may still cause the NLC particles to become more brittle and thus fragment more easily than pure ice particles.

To correctly interpret the MUDD data to obtain information on the MSP contribution, we need knowledge about to what extent the ice fragments will affect the observed current on BP. The key to answering this question lies in the fragmentation process. If the NLC/PMSE particles, even if they have up to a few percent of MSPs embedded by volume, behave like pure ice particles, they should primarily rebound

from the impact surface without severe fragmentation. Their probability of acquiring substantial charge is small and they will not contribute much to the current at BP. Smaller NLC/PMSE particles of sizes of several nm and below tend to stick to the surface and evaporate. They should therefore also not contribute much to the current at BP.[69–71]

If large ice particles, of say 50 nm, rebound and carry with them an initial charge of around $-4e$, they could only contribute a current of 4%–8% of the maximum current measured at BP. This follows from the results of Havnes *et al.*,[2] Havnes and Næsheim,[3] Kassa *et al.*[55] that an impacting 50 nm particle can typically produce 50–100 charged fragments. Even though fragmentation releasing small MPSs may seem to be required, large charged ice fragments may constitute a small part of the fragment currents in the highest energy ranges.

B. Detection limits for MUDD on PHOCUS

The BP voltage settings for the first MUDD launch were presented in Sec. II. The detecting scheme allowed for observation of fragments at three different BP voltages; two modes of retarding potentials between G2 and BP ($V_{BP} = -10$ V and $V_{BP} = 0$ V) and one with zero potential ($V_{BP} = +10$ V). During the time dust fragments are inside the probe, no significant evaporation from the MSP fragments is observed, even though the heating of these may be artificially high due to that the thermal radiation from grains has been neglected. Thus, we propose that the size distribution of measured fragments, presumably MSPs, is equal or very closely related to their true size distribution inside the NLCs.[1] On the basis of our simulations of spherical NLC fragments, we present in Table II the theoretical detection limits for pure ice fragments and MSPs in MUDD. Due to discussion above that ice particles of radii smaller than ~3 nm tend to stick impact surfaces and also experience a rapid evaporation, we have not included these in the mode with no retarding fields ($V_{BP} = +10$ V). The requirement for a significant detection is set to that 30% of the fragments of a given size will reach BP.

The dynamic shape of the particles, deflection angle from G2, as well as the uncertainty in MSP density are factors which will introduce shifts in the obtained size limits; however, these contributions will not be discussed in this paper. One particular factor which has not been included, but may become important is the transport of small fragments which stop between G2 and BP due to air drag. Our calculations predict that most MSP fragments with radii $\lesssim$0.6 nm will be stopped by neutral air drag between G2 and BP in the zero potential mode ($V_{BP} = +10$ V). Pure ice fragments of such sizes are found to evaporate fast and lose their charge; however, this should not be true for MSPs. Since the theoretical size distribution of MSPs predicts that they are abundant at small radii,[38,46] we must also consider their fate if they are stopped completely by neutral gas particles. A simple solution to this problem is that random walk processes move the fragments to whichever is closest of G2 and BP. For future probes, we will also include an accelerating potential between G2 and BP to ensure the detection of very small MSPs; however, this will also increase the free electron current which must be corrected for.[1]

TABLE II. Theoretical detection limits for the MUDD probe flown on PHOCUS in July 2011. EB denotes the error bound for the minimum detectable radius where [L,U] are the lower and upper limits due to an uncertainty of ± 100 ms^{-1} in initial fragment velocity.

	V_{BP} (V)	Mean (nm)	EB [L,U]
MSP	−10	1.8	[1.6, 2.2]
	0	1.5	[1.3, 1.8]
	+10	0.7	[0.6, 0.9]
ICE	−10	3.3	[3.0, 4.0]
	0	2.9	[2.5, 3.5]

C. Alternative potential modes

The MUDD probe as launched on the PHOCUS rocket in 2011[1] is a coarse mass spectrometer for charged dust or aerosol fragments. The mass resolution is dependent on the choice of retarding potentials between G2 and BP. The use of more potentials than in the first flight will, in principle, lead to a better resolution of the observed fragment energy spectrum, but the longer sweep time; this implies will reduce the height resolution. In a future flight of MUDD planned for 2015, we will use up to three mechanically identical MUDD probes which cycle through different sets of retarding potentials. The potential switching times will not be simultaneous so measurements from the different MUDDs will overlap. This will yield an increased accuracy and better spatial and energy resolution.

From the analysis of the first flight data from the MUDD probe, Havnes *et al.*[1] found that approximately 30% of the charged fragments, which were detected when the retarding potential between G2 and BP was zero, were stopped when the retarding potential was switched to 10 V. When the potential subsequently switched to 20 V, 50% were stopped. This implies that approximately 30% of the fragments were found to have energies below 10 eV, while 20% of fragments were found to have energies between 10 eV and 20 eV. The last 50% of the fragments, which have estimated energies $>$ 20 eV, were not stopped even by the largest potential. Large ice particles with masses up to the initial NLC mass may contribute to this current but should not dominate. We found for the ice fragments that particles with radii smaller than around 2.5 nm will not reach BP due to electrostatic forces, neutral gas friction, and evaporation. The previously discussed results from Kassa *et al.*,[55] Tomsic,[68] Adams and Smith,[77] and Friichtenicht[89] show that small ice fragments tend to stick to impact surfaces in a collision and moreover have a lower charging probability than MSPs. This suggests that the distinguishable BP currents in the modes with low potential is likely to be dominated by pure MSPs.

Figure 9 shows possible choices of retarding potentials in a future flight of MUDD, compared to the theoretical MSP size spectrum. The black lines give the choice of BP potentials (the corresponding retarding potentials being $V_{BP} = -10$ V) and indicate the minimum sizes which can be stopped by

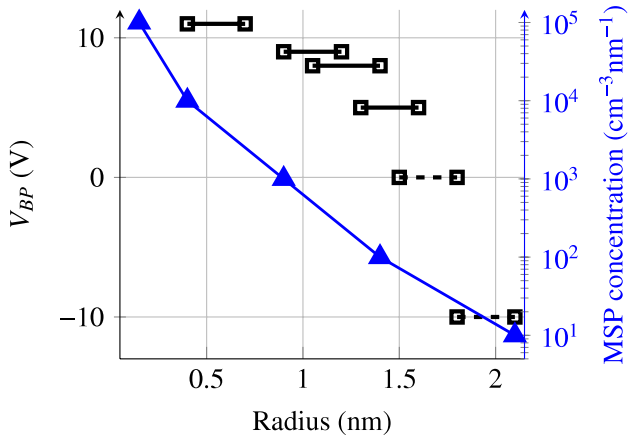

FIG. 9. Coverage of the theoretical MSP size spectrum with MUDD for an initial fragment velocity of 450 ms^{-1} (black with squares) with different retarding and accelerating potentials. The MSP spectrum (blue solid line) is the theoretical distribution at around 90 km.[38,52] The dashed lines represent the modes utilized in the PHOCUS campaign, July 2011.

those potentials. The uncertainties in the sizes are indicated by the horizontal extent of the lines. The upper limit of a size interval (squares) is the radius above which all charged fragments will contribute to the current in a certain mode. If the abundance of MSPs in the lower part of the spectrum implies that the concentration of these small MSPs is also present at large numbers inside NLC particles, there is a definite need to improve the resolution of MUDD and similar probes at low energies.

D. E-field edge effects

In the results from the fragment transport calculation presented here, we utilized an idealized electric field to reduce possible unrealistic numerical instabilities due to small fragments starting off in an extreme electric field. The electric field is observed to have values on the order of 10 000 Vm^{-1}, i.e., a decade higher than the infinite conducting plane solutions. However, these anomalies might not introduce unwanted effects, such as decelerating particles or deflecting them to the walls, because anomalous fields between G2 and BP are directed towards the probe in the modes with retarding potentials. Furthermore, the strong fields between the bucket and the outermost G2 ring will probably not represent the real fields, since G2 in reality is insulated from the bucket by a teflon ring which is not included in the simulations, and will probably reduce the outermost anomalies. For V_{BP} = +10 V, when the theoretical field is zero, the boundary effect might become important; in the regions below the two outermost rings of G2, the E-fields can become as large as ∼1000 Vm^{-1}, which is sufficient to significantly slow down or even stop small particles completely. If the particle flux through this region was effectively reduced, the current which we have regarded as the current due to all charged fragments will be reduced, possibly by a significant fraction. If this was the case, the total secondary charge production should be increased by a similar fraction. If the E-fields above and between the two outermost rings of G2 were to effectively shield out the charged fragments, the fraction would become just above 20%. Although the fields between G1 and G2 also have irregularities, the NLC particles are too energetic to be significantly affected.

VI. CONCLUSIONS

In this paper, we have studied the transport and dynamics of collision fragments created when mesospheric PMSE/NLC particles impact with an interior grid G2 on the rocket-borne MUDD probe, using computer simulations with a dedicated model. The model for dust fragment dynamics included the heating and evaporation of grains, and the model equations were closed by background simulations of the electric fields and neutral gas flow inside and around the probe. Our studies support the conclusion by Havnes *et al.*[1] Our simulations indicate that they observed MSP particles with radii >1.5 nm for a bottom plate potential of 0 V, >1.8 nm for a bottom plate potential of −10 V, and >0.6 nm for a bottom plate potential of +10 V. At radii above 1.8 nm and 2.1 nm in the two modes with V_{BP} = 0 V and V_{BP} = −10 V, respectively, all charged MSPs would reach BP. We observed a rapid evaporation of pure ice fragments, and when discussing our results in the light of the observations of pure ice particles by Tomsic,[68] Tomsic, Marković, and Pettersson,[69] Tomsic *et al.*,[70,71] and Andersson *et al.*,[72] e.g., that ice particles smaller than ∼3 nm tend to stick to impact surfaces, we conclude that few low energy ice fragments are observed in MUDD. The detection limit for ice fragments for the lowest potential mode is thus ∼3 nm and for the highest potential mode ∼3.5 nm. Finally, we find that ice fragments most likely contribute only a minor part of the observed energy spectrum. Since the MUDD probe from Havnes *et al.*[1] only contained the three discussed voltage modes, it is uncertain whether larger ice fragments contributed significantly to the BP current.

An uncertainty in initial fragment velocity of ±100 ms^{-1} is found to shift the observed size distribution of MSPs down between 0.2 and 0.3 nm and up between 0.3 and 0.4 nm; for ice fragments, these errors are slightly larger. The neutral gas fields inside the probe are found to brake/retard the smallest fragments to some extent. We have not considered the effect of local turbulence between G2 and BP, as the DSMC simulations[59] indicate no significant turbulent gas motion inside MUDD. Electric fields may however decrease the flux of small fragments near the edges of probes, as anomalous large fields can reduce the effective cross section of the G2 grid.

Even if MSPs carry small ice layers of up to 3 Å around them, they will have a very similar observed energy spectrum as the MSPs without ice, since the ice evaporates quickly. Our model does not include the heating of fragments during the fragmentation process; however, simple calculations of the contact heating during collision suggest that both ice fragments and MSPs at the surface of the NLCs are found to acquire significant heat at time scales on the order of 10^{-11} s. Such an initial heating strengthen our assumption that few small ice particles will be detected in MUDD. The MSPs are unaffected by this heating, since their acquired heat is not sufficient to cause significant evaporation. It is not improbable that an evaporating ice layer will reduce the friction on the

released MSPs, resulting in higher velocities than what we have used.

From our study of alternative potential modes in MUDD, we find a clear advantage in adding several new potential modes. These, together with more than one mechanically identical MUDD probes on future flights, will ensure a higher resolution and an improved accuracy of the lower part of the energy spectrum and thus, MSP fragments.

[1]O. Havnes, J. Gumbel, T. Antonsen, J. Hedin, and C. L. Hoz, J. Atmos. Sol.-Terr. Phys. **118**, 190 (2014).
[2]O. Havnes, T. Antonsen, T. Hartquist, Å. Fredriksen, and J. Plane, "The Tromsø programme of *in situ* and sample return studies of mesospheric nanoparticles," J. Atmos. Sol-Terr. Phys. (in press).
[3]O. Havnes and L. I. Næsheim, Ann. Geophys. **25**, 623 (2007).
[4]M. E. Hervig, L. E. Deaver, C. G. Bardeen, J. M. Russell III, S. M. Bailey, and L. L. Gordley, J. Atmos. Sol.-Terr. Phys. **84-85**, 1 (2012).
[5]G. E. Thomas, Rev. Geophys. **29**, 553, doi:10.1029/91RG01604 (1991).
[6]M. Hervig, R. E. Thompson, M. McHugh, L. L. Gordley, J. M. Russell, and M. E. Summers, Geophys. Res. Lett. **28**, 971, doi:10.1029/2000GL012104 (2001).
[7]B. Inhester, J. Klostermeyer, F. J. Lübken, and U. von Zahn, J. Geophys. Res.: Atmos. **99**, 20937, doi:10.1029/94JD01619 (1994).
[8]M. Rapp and F.-J. Lübken, Atmos. Chem. Phys. **4**, 2601 (2004).
[9]F.-J. Lübken and J. Höffner, Geophys. Res. Lett. **31**, L08103, doi:10.1029/2004GL019586 (2004).
[10]C. She, B. Williams, P. Hoffmann, R. Latteck, G. Baumgarten, J. Vance, J. Fiedler, P. Acott, D. Fritts, and F.-J. Lubken, J. Atmos. Sol.-Terr. Phys. **68**, 93 (2006).
[11]C. G. Bardeen, O. B. Toon, E. J. Jensen, D. R. Marsh, and V. L. Harvey, J. Geophys. Res. **113**, D17202, doi:10.1029/2007JD009515 (2008).
[12]M. E. Hervig, L. L. Gordley, L. E. Deaver, D. E. Siskind, M. H. Stevens, J. M. Russell III, S. M. Bailey, L. Megner, and C. G. Bardeen, Geophys. Res. Lett. **36**, L18805, doi:10.1029/2009GL039737 (2009).
[13]O. Havnes and M. Kassa, J. Geophys. Res.: Atmos. **114**, D09209, doi:10.1029/2008JD011276 (2009).
[14]M. J. Prather and J. Rodriguez, Geophys. Res. Lett. **15**, 1, doi:10.1029/GL015i001p00001 (1988).
[15]C. Voigt, H. Schlager, B. P. Luo, A. Dornbrack, A. Roiger, P. Stock, J. Curtius, H. Vossing, S. Borrmann, S. Davies, P. Konopka, C. Schiller, G. Shur, and T. Peter, Atmos. Chem. Phys. **5**, 1371 (2005).
[16]P. Keckhut, A. Hauchecorne, and M. L. Chanin, J. Geophys. Res.: Atmos. **100**, 18887, doi:10.1029/95JD01387 (1995).
[17]P. Keckhut, Adv. Space Res. **28**, 955 (2001).
[18]E. P. Shettle, M. T. DeLand, G. E. Thomas, and J. J. Olivero, Geophys. Res. Lett. **36**, L02803, doi:10.1029/2008GL036048 (2009).
[19]M. Gadsden, Adv. Space Res. **20**, 2097 (1997).
[20]G. Thomas and J. Olivero, Adv. Space Res. **28**, 937 (2001).
[21]M. Andreae and D. Rosenfeld, Earth-Sci. Rev. **89**, 13 (2008).
[22]U. von Zahn, Eos, TAGU **84**, 261 (2003).
[23]D. J. Cziczo, D. S. Thomson, and D. M. Murphy, Science **291**, 1772 (2001).
[24]E. K. Bigg, Meteorit. Planet. Sci. **47**, 799 (2012).
[25]O. Havnes, J. Trøim, T. Blix, W. Mortensen, L. I. Næsheim, E. Thrane, and T. Tønnesen, J. Geophys. Res.: Space Phys. **101**, 10839, doi:10.1029/96JA00003 (1996).
[26]L. J. Gelinas, K. A. Lynch, M. C. Kelley, S. Collins, S. Baker, Q. Zhou, and J. S. Friedman, Geophys. Res. Lett. **25**, 4047, doi:10.1029/1998GL900089 (1998).
[27]K. A. Lynch, L. J. Gelinas, M. C. Kelley, R. L. Collins, M. Widholm, D. Rau, E. MacDonald, Y. Liu, J. Ulwick, and P. Mace, J. Geophys. Res.: Space Phys. **110**, A03302, doi:10.1029/2004JA010502 (2005).
[28]M. Rapp, J. Hedin, I. Strelnikova, M. Friedrich, J. Gumbel, and F.-J. Lübken, Geophys. Res. Lett. **32**, L23821, doi:10.1029/2005GL024676 (2005).
[29]P. Schulte and F. Arnold, Geophys. Res. Lett. **19**, 2297, doi:10.1029/92GL02631 (1992).
[30]S. Robertson, M. Horanyi, S. Knappmiller, Z. Sternovsky, R. Holzworth, M. Shimogawa, M. Friedrich, K. Torkar, J. Gumbel, L. Megner, G. Baumgarten, R. Latteck, M. Rapp, U.-P. Hoppe, and M. E. Hervig, Ann. Geophys. **27**, 1213 (2009).
[31]M. Horanyi, J. Gumbel, G. Witt, and S. Robertson, Geophys. Res. Lett. **26**, 1537, doi:10.1029/1999GL900298 (1999).
[32]J. Hedin, J. Gumbel, and M. Rapp, Atmos. Chem. Phys. **7**, 3701 (2007).
[33]S. G. Love and D. E. Brownlee, Science **262**, 550 (1993).
[34]J. M. C. Plane, Chem. Soc. Rev. **41**, 6507 (2012).
[35]J. M. C. Plane, Chem. Rev. **103**, 4963 (2003).
[36]J. Höffner and J. S. Friedman, Atmos. Chem. Phys. **4**, 801 (2004).
[37]J. Rosinski and R. H. Snow, J. Meteorol. **18**, 736 (1961).
[38]D. M. Hunten, R. P. Turco, and O. B. Toon, J. Atmos. Sci. **37**, 1342 (1980).
[39]R. W. Saunders and J. M. Plane, J. Atmos. Sol.-Terr. Phys. **68**, 2182 (2006).
[40]J. M. Plane, J. Atmos. Sol.-Terr. Phys. **73**, 2192 (2011).
[41]M. Rapp and G. E. Thomas, J. Atmos. Sol.-Terr. Phys. **68**, 715 (2006).
[42]R. Turco, O. Toon, R. Whitten, R. Keesee, and D. Hollenbach, Planet. Space Sci. **30**, 1147 (1982).
[43]M. N. Eremenko, S. V. Petelina, A. Y. Zasetsky, B. Karlsson, C. P. Rinsland, E. J. Llewellyn, and J. J. Sloan, Geophys. Res. Lett. **32**, L16S06, doi:10.1029/2005GL023013 (2005).
[44]A. Y. Zasetsky, S. V. Petelina, and I. M. Svishchev, Atmos. Chem. Phys. **9**, 965 (2009).
[45]A. Evans, *The Dusty Universe*, Series in Astronomy (John Wiley & Sons, 1994), pp. 59–99.
[46]L. Megner, D. E. Siskind, M. Rapp, and J. Gumbel, J. Geophys. Res.: Atmos. **113**, D03202, doi:10.1029/2007JD009054 (2008).
[47]L. Megner, J. Gumbel, M. Rapp, and D. Siskind, Adv. Space Res. **41**, 41 (2008).
[48]B. J. Murray and E. J. Jensen, J. Atmos. Sol.-Terr. Phys. **72**, 51 (2010).
[49]G. von Cossart, J. Fiedler, and U. von Zahn, Geophys. Res. Lett. **26**, 1513, doi:10.1029/1999GL900226 (1999).
[50]C. von Savigny, C. E. Robert, G. Baumgarten, H. Bovensmann, and J. P. Burrows, Atmos. Meas. Tech. **2**, 523 (2009).
[51]L. Megner, M. Khaplanov, G. Baumgarten, J. Gumbel, J. Stegman, B. Strelnikov, and S. Robertson, Ann. Geophys. **27**, 943 (2009).
[52]L. Megner, M. Rapp, and J. Gumbel, Atmos. Chem. Phys. **6**, 4415 (2006).
[53]A. M. Zadorozhny, A. A. Vostrikov, G. Witt, O. A. Bragin, D. Y. Dubov, V. G. Kazakov, V. N. Kikhtenko, and A. A. Tyutin, Geophys. Res. Lett. **24**, 841, doi:10.1029/97GL50866 (1997).
[54]B. Smiley, M. Rapp, T. Blix, S. Robertson, M. Horányi, R. Latteck, and J. Fiedler, J. Atmos. Sol.-Terr. Phys. **68**, 114 (2006).
[55]M. Kassa, M. Rapp, T. W. Hartquist, and O. Havnes, Ann. Geophys. **30**, 433 (2012).
[56]T. A. Bekkeng, A. Barjatya, U.-P. Hoppe, A. Pedersen, J. I. Moen, M. Friedrich, and M. Rapp, Ann. Geophys. **31**, 187 (2013).
[57]See http://www.comsol.com/acdc-module for PDE module.
[58]A. Beskok and G. E. Karniadakis, J. Thermophys. Heat Transfer **8**, 647 (1994).
[59]G. Bird, *Molecular Gas Dynamics and the Direct Simulation of Gas Flows*, Oxford Science Publications (Oxford University Press, Incorporated, 1994).
[60]M. J. Baines, I. P. Williams, and A. S. Asebiomo, Mon. Not. R. Astron. Soc. **130**, 63 (1965).
[61]R. D. Smirnov, A. Y. Pigarov, M. Rosenberg, S. I. Krasheninnikov, and D. A. Mendis, Plasma Phys. Controlled Fusion **49**, 347 (2007).
[62]N. A. Fuchs, Q. J. R. Meteorol. Soc. **91**, 249 (1965).
[63]P. F. DeCarlo, J. G. Slowik, D. R. Worsnop, P. Davidovits, and J. L. Jimenez, Aerosol Sci. Technol. **38**, 1185 (2004).
[64]B. Rizk, D. M. Hunten, and S. Engel, J. Geophys. Res.: Space Phys. **96**, 1303, doi:10.1029/90JA01998 (1991).
[65]M. Podolak, J. B. Pollack, and R. T. Reynolds, Icarus **73**, 163 (1988).
[66]I. Strelnikova, M. Rapp, S. Raizada, and M. Sulzer, Geophys. Res. Lett. **34**, L15815, doi:10.1029/2007GL030635 (2007).
[67]J. M. C. Plane, Atmosp. Chem. Phys. **4**, 627 (2004).
[68]A. Tomsic, "Collisions between water clusters and surfaces," Ph.D. thesis (Göteborg University, 2001).
[69]A. Tomsic, N. Marković, and J. B. Pettersson, Chem. Phys. Lett. **329**, 200 (2000).
[70]A. Tomsic, P. U. Andersson, N. Markovic, W. Piskorz, M. Svanberg, and J. B. C. Pettersson, J. Chem. Phys. **115**, 10509 (2001).
[71]A. Tomsic, H. Schrder, K.-L. Kompa, and C. R. Gebhardt, J. Chem. Phys. **119**, 6314 (2003).
[72]P. U. Andersson, A. Tomsic, M. B. Andersson, and J. B. Petterson, Chem. Phys. Lett. **279**, 100 (1997).
[73]S. Sato, D.-R. Chen, and D. Y. Pui, Aerosol Air Qual. Res. **7**, 278 (2007).
[74]H. Kuuluvainen, A. Arffman, E. Saukko, A. Virtanen, and J. Keskinen, J. Aerosol Sci. **55**, 104 (2013).
[75]D. Dubov and A. Vostrikov, Journal of Aerosol Science **22**(1), S245 (1991), proceedings of the 1991 European Aerosol Conference Abstracts of the Nineteenth Annual Conference of the Gesellschaft für Aerosolforschung

e.V. Association for Aerosol Research Association Pour La Recherche des Aerosols.
[76]A. Vostrikov and D. Dubov, Z. Phys. D: At., Mol. Clusters **20**, 61 (1991).
[77]N. Adams and D. Smith, Planet. Space Sci. **19**, 195 (1971).
[78]P. Bliokh, V. Sinitsin, and V. Yaroshenko, *Dusty and Self-Gravitational Plasmas in Space*, Astrophys. Space Sci. Libr. (Springer, 1995).
[79]B. T. Draine and B. Sutin, Astrophys. J. **320**, 803 (1987).
[80]A. R. Klekociuk, P. G. Brown, D. W. Pack, D. O. ReVelle, W. N. Edwards, R. E. Spalding, E. Tagliaferri, B. B. Yoo, and J. Zagari, Nature **436**, 1132 (2005).
[81]H. Lichtenegger and N. Kömle, Icarus **90**, 319 (1991).
[82]J. Klinger, Icarus **47**, 320 (1981).
[83]B. Gundlach, S. Kilias, E. Beitz, and J. Blum, Icarus **214**, 717 (2011).
[84]L.-O. Heim, J. Blum, M. Preuss, and H.-J. Butt, Phys. Rev. Lett. **83**, 3328 (1999).
[85]M. Rapp, J. Gumbel, and F.-J. Lübken, Ann. Geophys. **19**, 571 (2001).
[86]F.-J. Lübken, J. Lautenbach, J. Höffner, M. Rapp, and M. Zecha, J. Atmos. Sol.-Terr. Phys. **71**, 453 (2009).
[87]N. Markovic, P. U. Andersson, M. B. Någård, and J. B. Pettersson, Chem. Phys. **247**, 413 (1999).
[88]M. Rapp, I. Strelnikova, B. Strelnikov, M. Friedrich, J. Gumbel, U.-P. Hoppe, T. Blix, O. Havnes, P. Bracikowski, K. Lynch, and S. Knappmiller, *Aeronomy of the Earth's Atmosphere and Ionosphere*, IAGA Special Sopron Book Series Vol. 2, edited by M. A. Abdu and D. Pancheva (Springer Netherlands, 2011), pp. 67–74.
[89]J. Friichtenicht, Nucl. Instrum. Methods **28**, 70 (1964).